(This is a sample cover image for this issue. The actual cover is not yet available at this time.)

Spectrochimica Acta Part A: Molecular and Biomolecular Spectroscopy 97 (2012) 830–837

Contents lists available at SciVerse ScienceDirect

Spectrochimica Acta Part A: Molecular and Biomolecular Spectroscopy

journal homepage: www.elsevier.com/locate/saa

Structure and UV-induced photochemistry of 2-furaldehyde dimethylhydrazone isolated in rare gas matrices

C. Araujo-Andrade [a], B.M. Giuliano [c], A. Gómez-Zavaglia [b,c,*], R. Fausto [c]

[a] Unidad Académica de Física de la Universidad Autónoma de Zacatecas, Zacatecas, Mexico
[b] Centro de Investigación y Desarrollo en Criotecnología de Alimentos (Conicet La Plata, UNLP), 1900 La Plata, Argentina
[c] Department of Chemistry, University of Coimbra, 3004-535 Coimbra, Portugal

HIGHLIGHTS

- The *E* forms of 2FDH have considerably lower energy than the *Z* forms.
- Both *E* conformers could be trapped in low temperature argon and xenon matrices.
- No conformational isomerization was observed upon annealing.
- UV irradiation induced (a) conformational isomerization of the *E* forms; (b) production of furan + dimethylisocyanide.

GRAPHICAL ABSTRACT

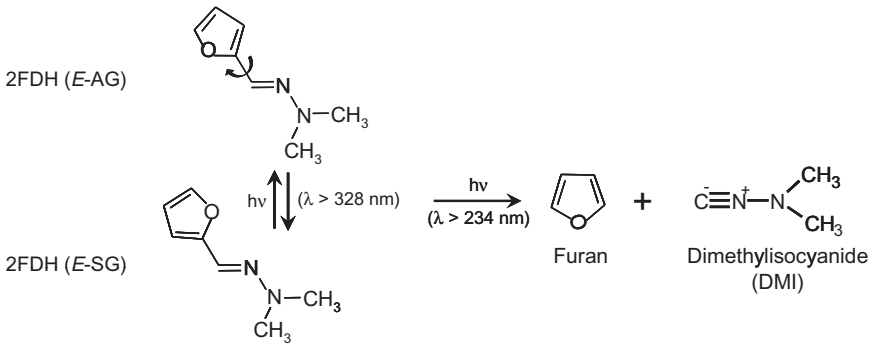

ARTICLE INFO

Article history:
Received 14 April 2012
Received in revised form 11 July 2012
Accepted 13 July 2012
Available online 25 July 2012

Keywords:
2-Furaldehyde dimethylhydrazone
Matrix isolation
Infrared spectroscopy
DFT(B3LYP)/6-311++G(d,p) calculations
Photochemistry

ABSTRACT

In this work, a combined matrix isolation FTIR and theoretical DFT(B3LYP)/6-311++G(d,p) study of 2-furaldehyde dimethylhydrazone (2FDH) was performed. According to calculations, two *E* and two *Z* conformers exist, the *E* forms having considerably lower energy than the *Z* forms. The absence of relevant sterical hindrance between the two substituents around the C=N bond (dimethylamino and 2-furyl) in the *E* structures and an extended π–p electron delocalization in the hydrazone moiety determines the higher stability of these species relatively to the *Z* structures. In the lowest energy form (*E*-AG) the O–C–C=N and C=N–N–Lp (Lp = lone electron pair of amine nitrogen atom) dihedral angles are predicted by the calculations to be −177.2° and 93.7°, respectively. The weak (N=C)–H···O hydrogen bond type interaction (H···O distance: 252.2 pm) in form *E*-AG, together with the absence in this form of the destabilizing interaction between the lone electron pairs of the oxygen and nitrogen atoms existing in *E*-SG, explains its lower energy in comparison with this latter form. Both *E*-AG and *E*-SG conformers could be trapped from room temperature gas phase in low temperature argon and xenon matrices. The high *E*-SG → *E*-AG energy barrier (>25 kJ mol^{-1}) explains that, upon increasing the temperature of the matrices no conformational isomerization could be observed. After irradiation of 2FDH with UV-light at $\lambda > 328$ and $\lambda > 234$ nm, two different photochemistries were observed. Irradiation at lower energy ($\lambda > 328$ nm) induced the *E*-AG → *E*-SG isomerization. Further irradiation at higher energy ($\lambda > 234$ nm) led to a quick consumption of 2FDH and production of furan and dimethylisocyanide.

Introduction

Hydrazones are organic compounds bearing the >C=N–N:< moiety, where the C=N double bond is conjugated with the lone electron pair (Lp) of the terminal nitrogen atom. This characteristic

* Corresponding author. Tel.: +54 91161756932.
E-mail address: angoza@qui.uc.pt (A. Gómez-Zavaglia).

1386-1425/$ - see front matter © 2012 Elsevier B.V. All rights reserved.
http://dx.doi.org/10.1016/j.saa.2012.07.061

structural feature determines in large extent the physical and chemical properties of hydrazones. Both nitrogen atoms of the hydrazone group are nucleophilic, the amino type nitrogen being more reactive. On the other hand, the carbon atom of the hydrazone group has both electrophilic and nucleophilic character, and hence, this is the most reactive hydrazone center [1–3]. The ability of hydrazones to react with both electrophilic and nucleophilic reagents broadens their applications in organic chemistry (*e.g.*, in condensation, cyclization and cycloaddition reactions for the synthesis of heterocycles) and in biotechnological and medical applications [1,4,5]. Several hydrazone derivatives have been reported as herbicides, insecticides, nematocides, rodenticides, plant regulators, as well as antituberculosis, spasmolytic and hypotensive agents. In addition, a number of hydrazones are also known to be active against leukemia, sarcoma and other malignant neoplasms and illnesses [5,6].

2-Furaldehyde dimethylhydrazone (2FDH; also known as furfural *N*,*N*-dimethylhydrazone, 2-furancarbaldehyde dimethylhydrazone, furan-2-carbaldehyde dimethylhydrazone or 2-furaldehyde 2,2-dimethylhydrazone) is a dimethylamino substituted hydrazone where the C atom is linked to a 2-furyl moiety. It can be synthesized from furfural and *unsym*-dimethylhydrazone [7], being mainly used in the chemical synthesis of furaldehyde derivatives [8] and many biologically active molecules relevant to the pharmaceutical industry, including trinitrophenyl, furylquinones and hydroquinones [9,10].

The >C═N–N:< group of hydrazones assumes in general a planar geometry, although the coplanarity may be broken down in certain sterically hindered molecules [11]. The length of the C═N bond depends on the nature of the substituents, varying from *ca.* 127 to 135 pm, but in all cases exceeding the values reported for aliphatic imines. The presence of the C═N double bond determines the existence of *E*–*Z* geometrical isomers in unsymmetrical hydrazones, like 2FDH. The presence of the >C═N–N:< group also makes hydrazones a convenient model for studying π–p conjugation [5]. This type of conjugation in hydrazones has been investigated spectroscopically by ultraviolet, Raman, infrared and nuclear magnetic resonance [5,12,13]. When conjugation is present, the electronic spectra of hydrazones show a bathochromic shift in the band corresponding to the lower energy $\pi \rightarrow \pi^*$ transition [14,15]. On the other hand, in the infrared spectra, π–p conjugation causes a redshift of *ca.* 70 cm^{-1} in the C═N stretching frequency, compared to that observed for aliphatic imines (1620–1590 cm^{-1} *vs* 1670–1650 cm^{-1}) [5,15]. In addition, the increase in the intensity of the C═N stretching Raman band on passing from unsubstituted hydrazones to alkylhydrazones has also been attributed to π–p conjugation [5,16].

Two types of photochemical reactions have been described for hydrazones: (a) nitrogen–nitrogen bond cleavage, and (b) if hydrogens are available at the terminal nitrogen, hydrogen migration from nitrogen to carbon. For some unsubstituted hydrazones, this second process results in a photochemical reaction resembling the Wolff–Kishner reduction [17,18]. When reactions take place in solution, the participation of solvent molecules and cross reactions involving initially formed intermediates generated from different reactant molecules make these reactions mechanistically complex. Indeed, hydrazones are known to show a great trend to be involved in bimolecular reactions (*e.g.*, cycloadditions and condensations) [1,4]. In this regard, isolation of the reactant molecules in a cryogenic inert matrix, avoiding by this way molecular diffusion to take place and bimolecular encounters, appears as an appropriate technique to shed light on the primary unimolecular photochemical processes. This approach was used in this work to investigate the details of the photochemistry of monomeric 2FDH. The compound was isolated in argon and xenon matrices, irradiated by UV light of different wavelengths, and the photoreactions probed by infrared spectroscopy. Interpretation of the experimental results were supported by theoretical calculations undertaken at the DFT(B3LYP)/6-311++G(d,p) level of approximation. The obtained results allowed also for detailed characterization of the potential energy surface landscape of the compound, and interpretation of its infrared spectra in both argon and xenon matrices.

Experimental and computational methods

Furfural *N*,*N*-dimethylhydrazone was obtained from Sigma–Aldrich (97% purity). Infrared spectra were obtained using a Nicolet 6700 FTIR spectrometer equipped with a deuterated triglycine sulfate (DTGS) detector and a Ge/KBr beamsplitter, with 0.5 cm^{-1} spectral resolution. In order to avoid interference from atmospheric H_2O and CO_2, a stream of dry/CO_2-filtered air continuously purged the optical path of the spectrometer. Matrices were prepared by co-deposition of 2FDH vapors coming out from a glass tube container coupled to the cryostat through a flux-controlling valve kept at room temperature, together with a large excess of the matrix gas (argon N60 or xenon N48, both supplied by Air Liquide) onto the CsI substrate of the cryostat cooled to 14 K (for argon) or 20 K (xenon). All experiments were performed using an APD Cryogenics closed-cycle helium refrigeration system with a DE-202A expander.

In situ UV irradiation of the matrices was carried out with UV light produced by a 500 W Hg(Xe) lamp (Newport, Oriel Instruments), with output power set to 200 W, through the outer KBr window of the cryostat. The irradiation has been performed using a long-pass optical filter transmitting UV light with $\lambda > 328$ nm, as well as with the unfiltered UV-light (*i.e.*, with $\lambda > 234$ nm; this wavelength value is defined by the absorbance edge of KBr in the UV).

The quantum chemical calculations were performed with Gaussian 03 [19] at the DFT level of theory, using the 6-311++G(d,p) basis set and the B3LYP functional, which includes Becke's gradient exchange correction [20] and the Lee, Yang and Parr correlation functional [21]. Structures were optimized using the Geometry Direct Inversion in the Iterative Subspace (GDIIS) method [22,23], and the nature of the resulting stationary points on the potential energy surface was determined by inspection of the corresponding calculated Hessian matrix. In order to assist the analysis of the experimental spectra, vibrational frequencies were calculated at the same level of theory. The computed harmonic frequencies were then scaled by a single factor (0.978) to correct them mainly for the effects of basis set limitations, neglected part of electron correlation and anharmonicity effects. The theoretical normal modes were analyzed by carrying out the potential energy distribution (PED) calculations, performed according to the procedure described in Ref. [24]. Cartesian harmonic force constants resulting from the DFT(B3LYP)/6-311++G(d,p) calculations were transformed into the force constants with respect to molecule fixed internal coordinates chosen as recommended by Pulay et al. [25]. Potential energy profiles for internal rotation were calculated by performing relaxed scans on

Table 1
DFT(B3LYP)/6-311++G(d,p) calculated relative energies (including zero point vibrational contribution) and predicted room temperature gas phase equilibrium populations for the two *E*-2FDH conformers.[a]

Conformer	ΔE_{ZPE}	Population (%)
E-AG	0.0 (−1200864.6)[b]	80.5
E-SG	3.5	19.5
Z-AG	26.7	
Z-SG	33.3	

[a] Energies in kJ mol^{-1}; conformers are depicted in Fig. 1.
[b] Total energy for *E*-AG′, with zero point vibrational energy contribution.

the PES along the relevant reaction coordinates, and the transition state structures for the conformational interconversions were obtained using the Synchronous Transit-Guided Quasi-Newton (STQN) method [26,27].

Results and discussion

2FDH potential energy surface landscape

In 2FDH, the relative position of the furyl and $N(CH_3)_2$ substituents around the C=N bond leads to *E* and *Z* isomerism. In addition, two rotational axes (O–C–C=N and C=N–N–Lp; Lp = lone electron pair of nitrogen atom) exist, which can give rise to conformational isomers. After a full search on the DFT(B3LYP)/6-311++G(d,p) potential energy surface of the molecule, four different minima were found: *E*-AG, *E*-SG, *Z*-AG and *Z*-SG, with zero point corrected relative energies of 0.0, 3.5, 26.7 and 33.3 kJ mol^{-1}, respectively (Table 1 and Fig. 1)[1]. All conformers belong to the C_1 point group and possess a symmetry equivalent structure. The calculated structural parameters for all the four conformers of 2FDH are provided in Table S1 (Supplementary material).

According to calculations, *E*-AG is the global minimum. In this form, the O–C–C=N and C=N–N-Lp dihedrals are equal to −177.2° and 93.7°, respectively. The slightly higher stability of the *E*-AG form relatively to *E*-SG (see Fig. 1) can be explained considering: (a) the presence of a stabilizing weak (N=C–H)···O hydrogen bond type interaction (H···O distance: 252.2 pm) and (b) the absence the destabilizing interaction between the lone

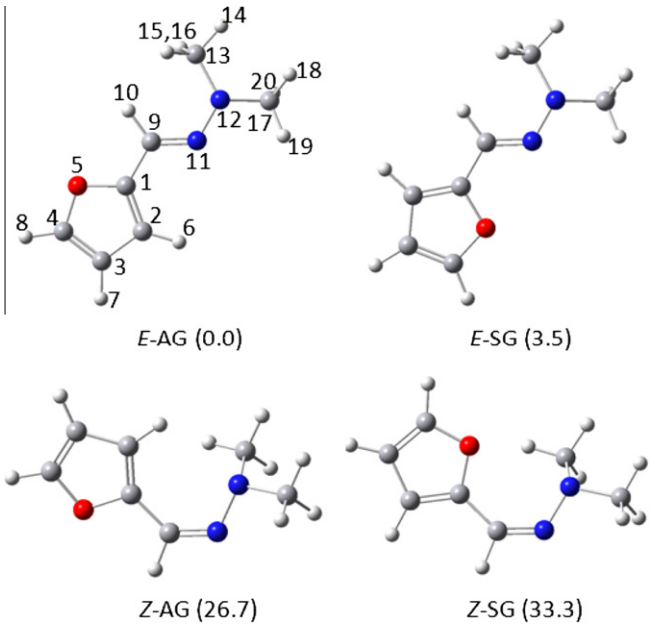

Fig. 1. DFT(B3LYP)/6-311++G(p,d) optimized geometries of the minimum energy structures of 2FDH. Relative energies (including zero point correction; in kJ mol^{-1}) are provided in parentheses.

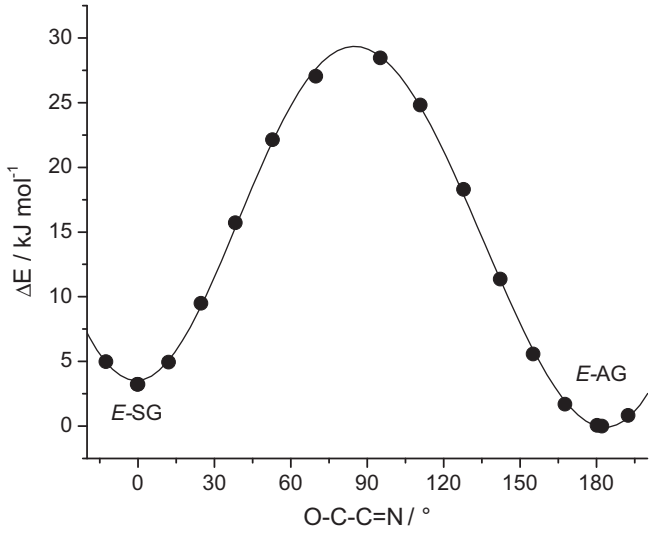

Fig. 2. DFT(B3LYP)/6-311++G(d,p) calculated potential energy profile for conformational interconversion between the *E*-AG and *E*-SG conformers of 2FDH.

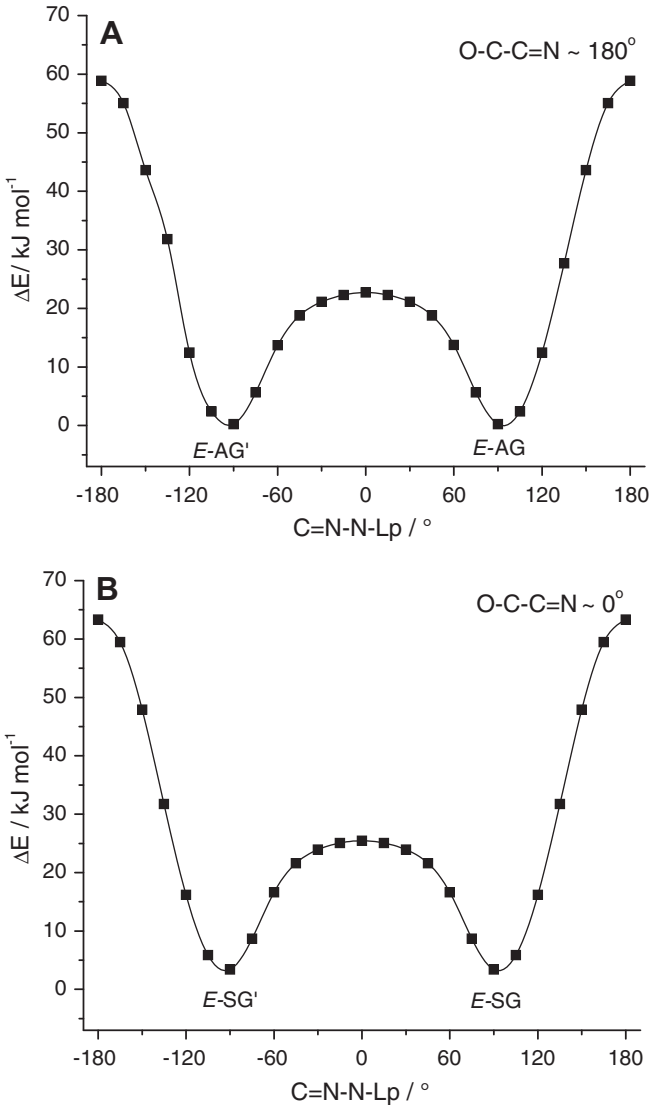

Fig. 3. DFT(B3LYP)/6-311++G(d,p) calculated potential energy profile for internal rotation around the N–N bond in *E*-2FDH: (A) for O–C–C=N ~ 180°; (B) for O–C–C=N ~ 0°. *E*-AG′ and *E*-SG′ are the symmetry-equivalent structures to *E*-AG and *E*-SG, respectively.

[1] The following criterion has been followed to assign names to the different minimum energy structures of 2FDH: the first letter indicates the orientation of the furyl and $N(CH_3)_2$ substituents with regard to the C = N bond (*E* = *entgegen*, 180°; *Z* = *zusammen*, 0°), the conformation defined by the O–C–C = N dihedral angle relates to the second letter (A = *anti*, 180°; S = *syn*, 0°), and that defined by the C = N–N–Lp dihedral angle determines the third letter (G = *gauche*, *ca.* 40-90°).

electron pairs of the oxygen and nitrogen atoms existing in *E*-SG. The *Z*-type structures (*Z*-AG and *Z*-SG) have a considerably higher energy than the *E* forms because of the sterical hindrance between the furyl and $N(CH_3)_2$ substituents (see Fig. 1) and the reduced π–p mesomerism (the C═N–N–Lp dihedrals in *E* and *Z* forms are *ca.* 90° and 50°, respectively). The estimated room temperature gas phase equilibrium populations of the two *E*-type conformers are 80.5%, for *E*-AG, and 19.5%, for *E*-SG.

Fig. 2 depicts the B3LYP/6-311++G(d,p) calculated potential energy profile for interconversion between the two conformers of

Table 2
Observed wavenumbers (ν, cm^{-1}) for 2FDH isolated in argon and xenon matrices and DFT(B3LYP)/6-311++G(d,p) calculated wavenumbers and intensities (I, km mol^{-1}) for conformers *E*-AG and *E*-SG.[a]

Approximate description	Calc.		Calc.		Exp. (Ar 14 K)		Exp. (Xe 20 K)	
	E-AG		*E*-SG		*E*-AG	*E*-SG	*E*-AG	*E*-SG
	ν[b]	I[c]	ν[b]	I[c]	ν	ν	ν	ν
$\nu(C_4–H_8)$	3207.4	0.0	3206.4	0.0	n.o.	n.o.	n.o.	n.o.
$\nu(HC_2C_3H)$s	3190.2	0.2	3167.2	1.5	n.o.	3127	n.o.	3120
$\nu(HC_2C_3H)$as	3170.1	4.6	3178.6	0.1	3127	3149	3120	3149
$\nu(CH_3)$as′ (1)			3070.2	2.0		3010		3003
$\nu(CH_3)$as″ (1)	3068.0	9.6	3054.7	2.8	3010	3000	3003	2993
$\nu(CH_3)$as″ (2)	3055.4	9.7			3000		2993	
$\nu(C_9–H_{10})$	3042.9	6.3	3033.5	6.8	2997	2997	2985	2985
$\nu(CH_3)$as′ (1), ν (CH_3)as′ (2)	3007.4	28.7			2966/2957		2951	
$\nu(CH_3)$as″ (2), ν (CH_3)as″ (1)			3005.9	7.4		2925		2917
$\nu(CH_3)$as′ (2), ν (CH_3)as′ (1)	2993.2	17.8	2991.5	4.5	2925	2925	2917	2917
$\nu(CH_3)$s (1)	2902.1	30.6	2902.0	122.4	2896/2875/2864/2861	2896/2875/2864/2861	2884/2866/2856	2884/2866/2856
$\nu(CH_3)$s (2)	2890.1	40.2	2888.5	10.5	2844/2834	2797/2792/2785	2836/2827	2796/2786/2779
ν(C═N)	1604.7	52.2	1619.8	11.9	1592/1589/1586/1584	1614	1590/1588/1581	1613
$\nu(C_1=C_2)$, $\nu(C_3=C_4)$	1575.9	0.2	1555.6	1.9	1553	1531	1555	1520
$\nu(C_3=C_4)$, δ (CH_3)as′ (1)			1488.2	8.7		1496/1493/1492/1489 (sh)		1496 (sh)/1493/1492/1488 (sh)
$\delta(CH_3)$as″ (1), $\nu(C_3=C_4)$	1485.1	28.8			1480/1471		1476/1468	
$\delta(CH_3)$as″ (1)	1480.1	18.2	1452.4	3.4	1466	1446 (sh)	1463/1461	1441
$\delta(CH_3)$as′ (1)	1471.9	8.6	1476.3	1.8	1456	1466	1457	1463/1461
$\delta(CH_3)$as′ (2)			1472.5	3.2		1460		1458 (sh)
$\delta(CH_3)$as″ (2), $\delta(CH_3)$as′ (2)	1453.4	17.7			1449		1444	
$\delta(CH_3)$as″ (2)	1450.3	7.6	1450.8	2.1	1446 (sh)	1446 (sh)	1441	1441
$\delta(CH_3)$s (1)	1429.1	2.1	1425.2	1.3	1423	1422	1421	1419
$\delta(CH_3)$s (2)	1406.1	4.9	1404.3	0.5	1404	1398	1401	1397
$\nu(C_2–C_3)$, $\delta(CCH_8)$, $\delta(HC_2C_3H)$as	1388.6	7.7	1388.1	0.3	1388	1387	1385	1382 (sh)
$\delta(C_1C_9H_{10})$, $\delta(C_1C_9=N)$			1350.4	8.4		1349		1349 (sh)
$\nu(C_2–C_3)$, $\delta(C_1C_9H_{10})$	1349.2	21.8			1349		1346/1345	
$\gamma(CH_3)''$ (1)	1128.8	39.5	1284.9	13.1	1134	1286	1130	1286
$\gamma(CH_3)'$ (1)	1278.0	63.9	1129.0	8.1	1280/1277	1135	1278/1275	1135/1133
δ(CNC)as, $\gamma(CH_3)''$ (1)			1265.6	7.1		1270		1265
δ(CNC)as	1257.2	10.6			1263		1260	
δ(CNC)as, $\nu(C_1–C_9)$			1244.0	0.6		1236		1232
$\delta(HC_2C_3H)$s, $\nu(C_1–C_9)$, $\delta(CCH_8)$	1229.5	2.7			1235		1232	
$\delta(HC_2C_3H)$s			1208.6	0.1		1204		1203
$\nu(O_5–C_1)$	1182.2	2.5			1201/1199 (sh)/1192/1190		1198/1197(sh)/1187/1186	
$\nu(C_4–O_5)$, $\delta(CCH_8)$			1149.8	2.4		1149		1149
$\delta(CCH_8)$, $\nu(C_4–O_5)$	1143.3	7.5			1137 (sh)		1136	
$\gamma(CH_3)'$ (2)	1029.0	8.7	1086.5	0.5	1032	1093	1036.1035	1090
$\gamma(CH_3)''$ (2)	1086.1	2.2	1028.9	2.3	1092	1020	1087	1020
$\nu(C_4–O_5)$	1082.6	1.6	1078.0	2.7	1085/1084	1080/1078	1083	1077
ν(N–N)	1038.3	158.4	1042.6	34.5	1038 (sh)/1037	1043/1042 (sh)	1041	1043 (sh)
$\nu(C_2–C_3)$, $\delta(HC_2C_3H)$as			1010.7	7.3		1015/1014		1014/1011
$\delta(HC_2C_3H)$as/s, $\nu(C_2–C_3)$	1003.2	25.0			1010/1008		1008/1006	
$\nu(O_5–C_1)$	953.1	4.9	930.6	4.7	961/959/954	938/937/935	961/958	939/936/934
δ(ring 2)	883.1	5.7	882.9	1.7	885	885	877	877
$\gamma(CH_{10})$	880.8	18.7	881.8	5.1	869	872	869 (sh)/866	875
$\gamma(HC_2C_3H)$as	858.7	0.2	852.4	0.1	859	858	859	858
ν(CNC)s	842.4	19.8	849.8	3.1	853/851	856	856/854/850/849	858
$\gamma(HC_2C_3H)$s	797.6	13.3	783.6	2.7	805/801/800/798	788	800/798/797	785
ν(CNC)s, δ(ring 1)	769.2	15.5	770.8	3.8	777	777	776	776
$\gamma(CH_8)$	714.3	51.3	720.9	13.5	727 (sh)/725/724 (sh)	732/731/729	724/723	729/728/727
ν(ring 2)	661.5	0.9	673.5	0.3	663	673	663	677
ν(ring 1)	592.7	5.9	592.0	1.6	596	594	594	592
tw$[N(CH_3)_2]$	532.9	14.2	532.9	3.3	539	539	539/537/535	539/537/535
$\delta[N(CH_3)_2]$	475.1	5.3	477.8	1.1	477	486/483	477	483

[a] ν, stretching; δ, bending; γ, rocking; τ, torsion; tw, twisting; s, symmetric; as, antisymmetric; n.o., not observed; sh. shoulder. See Tables S2–S6 for definition of internal coordinates and normal coordinate analysis.
[b] Calculated wavenumbers were scaled by 0.978.
[c] Calculated intensities were scaled by the calculated relative fractional populations in gas phase equilibrium at room temperature (0.8 for *E*-AG and 0.2 for *E*-SG).

E-2FDH. Note that despite the smaller energy difference between the two conformers (3.5 kJ mol^{-1}), the energy barriers for both the direct and reverse reactions are larger than 20 kJ mol^{-1}. Fig. 3 presents the calculated potential energy profiles for internal rotation about the N–N bond in *E*-2FDH, assuming the O–C–C=N dihedral angle in the *anti* (Fig. 3A) and *syn* (Fig. 3B) conformations. These plots show the pathways for interconversion between the two equivalent-by-symmetry pairs of *E*-type conformers. In both cases, the lower barrier occur for a conformation where the N lone electron pair is directed towards H_{10} (*ca.* 25 kJ mol^{-1}), while the most energetically demanding pathway has a transition state structure where the lone electron pairs of the two nitrogen atoms are aligned (*ca.* 60 kJ mol^{-1}). As it could be anticipated, in both transition state structures the π–p mesomerism within the hydrazone group is minimized.

IR spectra of matrix-isolated 2FDH

2FDH has 54 fundamental vibrations. For all minimum energy structures (*E*-AG, *E*-SG, *Z*-AG and *Z*-SG) all fundamental vibrations are predicted to be active in the infrared. Table S2 displays the definition of the internal coordinates used in the normal coordinate analysis undertaken in this study. The DFT(B3LYP)/6-311++G(d,p) calculated vibrational spectra for the different minima of 2FDH and the results of the normal coordinate analysis are given in Tables S3–S6. Table 2 shows the assignments for the experimental spectra of 2FDH in argon and xenon matrices.

Fig. 4 depicts the as-deposited spectra of 2FDH in argon and xenon matrices. The calculated spectra for conformers *E*-AG and *E*-SG are also shown in this figure (both as stick spectra and simulated by means of Lorentzian functions). In the calculated spectra, the intensities were scaled by the estimated relative populations of the *E*-AG and *E*-SG forms in the gas phase equilibrium at room temperature, based on their calculated relative energies (see Table 1). As it can be noticed, the theoretical spectra fit nicely the experimentally obtained ones, testifying the presence of both *E*-AG and *E*-SG isomers in the matrices with relative populations matching well the theoretical predictions based on the DFT calculations. Indeed, the relative populations of *E*-AG and *E*-SG could also be estimated from the experimental data. The two conformers give rise to a well separated pair of bands, at *ca.* 959 (*E*-AG) and 937 (*E*-SG) cm^{-1}, ascribed to the $\nu O_5–C_1$ vibration (calculated frequencies: 953.1 and 930.6 cm^{-1}, for *E*-AG and *E*-SG, respectively). From the relative integral intensities of the $\nu O_5–C_1$ observed bands due to the *E*-AG and *E*-SG conformers, divided by the corresponding calculated IR intensities, the relative amounts of the two forms present in the matrices could then be determined. The obtained *E*-AG:*E*-SG population ratios were 4.5:1, in xenon, and 6.1:1 in argon, in excellent agreement with the calculated theoretical populations. Moreover, annealing of the matrices above *ca.* 40 K also did not promoted any spectral change ascribable to conformational isomerization (above this temperature aggregation starts to take place). Such results indicate that the barriers for conformational isomerization are, in consonance with the theoretical predictions, at least higher than *ca.* 12 kJ mol^{-1} [28]. Indeed, according to the Barnes relationship [28], a temperature higher than *ca.* 80 K should be attained to overcome the ~25 kJ mol^{-1} barrier calculated for the *E*-SG → *E*-AG isomerization (see Fig. 2).

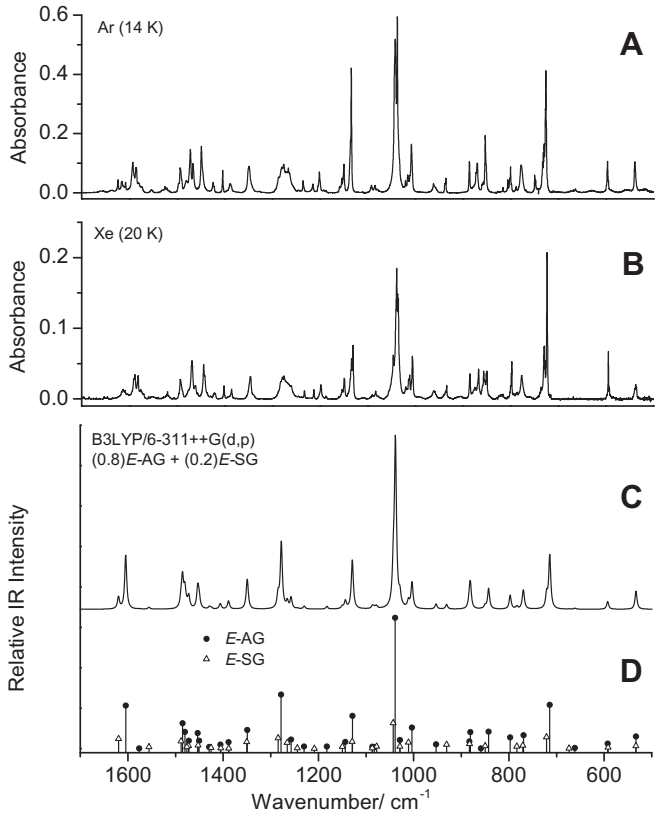

Fig. 4. Infrared spectra of 2FDH in argon (A) and xenon (B) matrices, obtained immediately after deposition at 14 and 20 K, respectively, B3LYP/6-311++G(d,p) calculated spectra for *E*-AG and *E*-SG conformers (C) and simulated theoretical spectrum of the conformational mixture (D). In the theoretical spectra, intensities were scaled by the equilibrium fractional relative populations of the conformers in gas phase at 298 K.

Photochemistry of matrix-isolated 2FDH

Upon broadband UV irradiation with UV-filtered light ($\lambda > 328$ nm) of argon and xenon matrix-isolated monomeric 2FDH, *E*-AG → *E*-SG conformational isomerization was observed, as noticed by the change in the relative intensities of the bands ascribed to the individual conformers. The bands ascribable to *E*-SG clearly increase, while those due to *E*-AG decrease. After 30 min irradiation, the population ratios of *E*-AG and *E*-SG obtained from the $\nu O_5–C_1$ experimental bands intensities changed from 4.5:1 to 3.3:1 in xenon, and from 6.1:1 to 2.1:1 in argon. In other words, the increase in the population of *E*-SG ranged 5–15%, being more extensive in argon matrix. These results are illustrated in Fig. 5, where the positive bands correspond to the less stable conformer *E*-SG, produced at expenses of the more stable *E*-AG form (negative bands). No 2FDH fragmentation nor *E* → *Z* structural isomerization (the last type of process has been observed frequently for hydrazones in solution either chemically or photochemically induced [29,30]), have been detected upon irradiation in these conditions.

After subsequent irradiation of the matrices with higher energy ($\lambda > 234$ nm), the spectrum of 2FDH lost intensity, whereas new bands developed, indicating the formation of new species (Fig. 6). In Fig. 6, the negative bands correspond to the consumed reagent (*E*-AG and *E*-SG conformers) and the positive ones to the obtained photoproducts. The bands emerging upon irradiation (both in argon and xenon matrices) can be doubtlessly assigned to furan and dimethylisocyanide (DMI), which can be formed from 2FDH by cleavage of the exocyclic C–C bond accompanied by [1,2] H-atom shift. *E* → *Z* structural isomerization of 2FDH was not observed in this case as well. A schematic picture of the observed photoprocess is shown in Fig. 7.

The assignment of the bands due to photoproducts is given in Table 3. This assignment has been performed taking into account the theoretically calculated infrared spectra of furan and DMI,

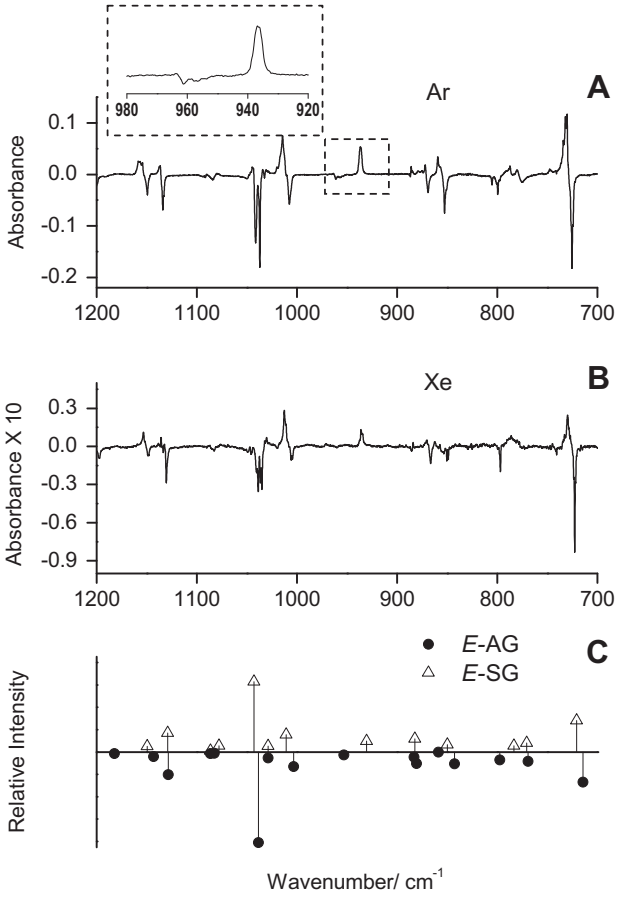

Fig. 5. Infrared difference spectra, irradiated matrix ($\lambda > 328$ nm; 30 min) *minus* as-deposited matrix. Positive bands correspond to *E*-SG conformer and negative bands to *E*-AG. (A and B) Experimental results in argon and xenon matrices and (C) calculated. In script A, a zoom of the 980–920 cm^{-1} region is shown in the dashed frame.

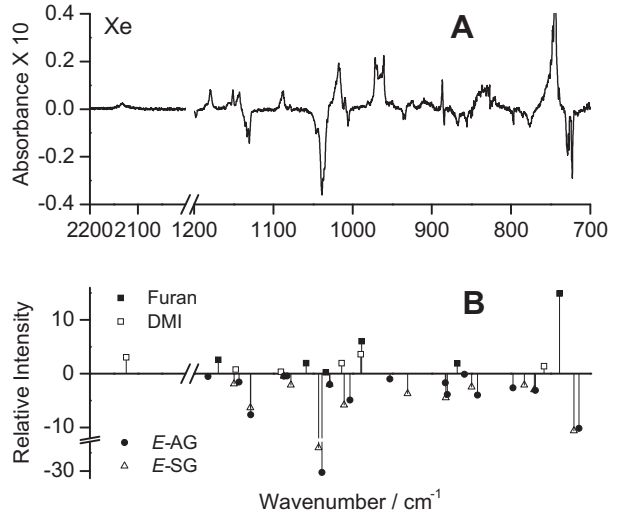

Fig. 6. (A) Infrared difference spectrum, irradiated xenon matrix ($\lambda > 234$ nm; 15 min) *minus* as-deposited matrix. Positive bands correspond to photoproduced species; negative to the reactant. (B) DFT(B3LYP)/6-311++G(d,p) calculated spectra (with wavenumbers scaled by 0.978) for the photoproducts (furan and dimethylisocianyde – DMI; bands pointing upwards) and 2FDH (*E*-AG and *E*-SG forms; bands pointing downwards).

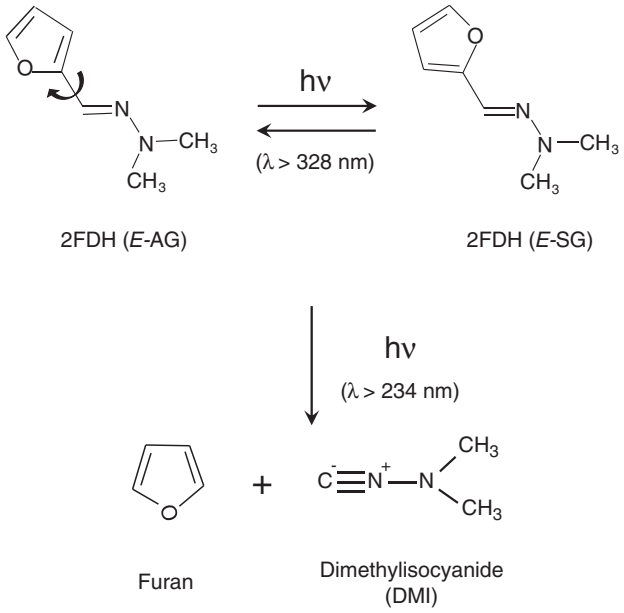

Fig. 7. Observed photoprocesses resulting from UV-irradiation of monomeric 2FDH isolated in argon and xenon matrices.

and also the previously reported experimental data for furan and isocyanides isolated in rare gas matrices [31–36].

Furan has been studied in cryogenic matrices before [31–35] and its identification as a photoproduct of 2FDH upon irradiation at $\lambda > 234$ nm could be easily performed. The most intense bands due to furan are due to one of the in-plane δ(C–H) bending modes and the all- in-phase out-of-plane γ(C–H) vibration, and have been ascribed previously for the compound in argon matrix at *ca.* 995 and 745 cm^{-1} [31–33]. The B3LYP/6-311++G(d,p) calculated frequencies for these two modes are 989 and 739 cm^{-1}, respectively. In the photolyzed 2FDH argon matrix, the corresponding bands are observed at 963 and 734/732/730 cm^{-1} (site splited feature), which have counterparts in the photolyzed xenon matrix at 960 and 750–744 cm^{-1} (structured band with several components resulting from site splitting). The small frequency shifts of the bands observed in the present study compared to the literature values result from the fact that in the present case the furan molecule is formed together with DMI and the two molecules shall interact in some extent in the matrix cage where they co-exist. Other bands of furan having lower intensities could also be identified in the spectra of the photolyzed matrices (see Table 3). There is no experimental evidence of subsequent photocleavage of the furan ring under the used experimental conditions.

Identification of DMI as photoproduct of 2FDH was facilitated by observation of the characteristic band due to the isocyanide stretching vibration at 2124 cm^{-1} (in argon matrix; 2132 cm^{-1}, in xenon). Isocyanides (or isonitriles) are organic isomers of cyanides (or nitriles), and are widely used in organic synthesis [37]. The high reactivity of isocyanides makes difficult their investigation at room temperature, but some of these compounds have been successfully isolated in rare gas matrices [36]. The ν(N≡C) vibration in matrix-isolated isocyanides have been observed in a characteristic frequency range (2200–2080 cm^{-1}) which is red-shifted regarding the usual frequency range for the same vibration in the corresponding cyanides (2300–2200 cm^{-1}) [36]. Most of the remaining bands expected to occur in the investigated spectral range for DMI could also be observed in the photolyzed 2FDH matrices (see Table 3 and also Fig. 6).

Table 3
Calculated IR spectra for the observed photoproducts ($\lambda > 234$ nm) of matrix-isolated 2FDH in argon and xenon and assignments for the experimentally observed bands.[a]

Assignment[b]	Calculated		Experimental		Ref. [31][c]
	Wavenumber	IR Intensity	Argon	Xenon	
Furan					
$\nu(C_\alpha{-}H)s$	3210.7	0.1	n.o.	n.o.	
$\nu(C_\alpha{-}H)as$	3204.5	0.2	n.o.	n.o.	
$\nu(C_\beta{-}H)s$	3180.4	0.2	n.o.	n.o.	
$\nu(C_\beta{-}H)as$	3170.0	2.5	n.o.	n.o.	
νC=C)as	1553.7	0.02	n.o.	1562	
νC=C)s	1473.2	20.9	1490/1480	1479/1478	
νC–C)	1377.6	2.8	1343	1339	
δC–H) (++++)	1255.8	0.1	n.o.	n.o.	
νC–O–C)as	1169.4	20.5	1181	1179	1177.7
δC–H) (+–+–)	1136.8	0.1	1145	1142	
δC–O)s	1058.7	15.4	1043	1043	1065.0
δC–H) (+––+)	1033.9	1.7	1020	n.o.	
δC–H)(++––)	989.0	47.9	963	960	993.6
δC=C–C)	873.5	0.8	870	n.o.	
δC–O–C)s	868.0	14.8	869	887	869.1
γC–H) (+–+–)	860.4	0.0	859	n.o.	
γC–H) (+––+)	831.4	0.0002	837(?)	830(?)	
γC–H) (++++)	738.8	117.3	734/732/730	750/748/747/745/744	744.1
γC–H) (++––)	715.7	0.0	n.o.	n.o.	
δ ring (butterfly)	604.6	24.9	595	596	603.3/602.3
δ ring (crawl)	596.0	0.0	n.o.	n.o.	
DMI					
$\nu(CH_3)as''$ (s)	3072.3	13.3	2973	3012	
$\nu(CH_3)as''$ (as)	3069.7	6.6	2973	3012	
$\nu(CH_3)as'$ (s)	3031.1	29.8	2940	2959	
$\nu(CH_3)as'$ (as)	3028.6	4.3	2940	2959	
$\nu(CH_3)s$ (s)	2927.5	81.5	2908	2900	
$\nu(CH_3)s$ (as)	2924.0	29.3	2869/2861	2871/2861	
ν(N≡C)	2124.3	23.9	2124	2132	
$\delta(CH_3)as''$ (s)	1477.4	18.3	1495	1483	
$\delta(CH_3)as''$ (as)	1462.2	1.6	1461	n.o.	
$\delta(CH_3)as'$ (s)	1459.8	19.9	1459	1465	
$\delta(CH_3)as'$ (as)	1447.4	10.6	1443	1453	
$\delta(CH_3)s$ (s)	1431.4	0.4	1421	1433	
$\delta(CH_3)s$ (as)	1408.6	0.0	1402	n.o.	
νN–N, νCNC)s	1245.2	2.0	1238	1235	
νCNC)as	1218.2	3.0	1230	1227	
$\gamma(CH_3)'$ (s)	1147.8	6.0	1156	1151	
$\gamma(CH_3)'$ (as)	1090.4	3.1	1090	1087/1088/1091	
$\gamma(CH_3)''$ (as)	1013.6	15.0	1017/1014	1017	
$\gamma(CH_3)''$ (s)	989.6	28.2	973/967	971/970	
ν(CNC)s, νN–N	758.3	10.9	750/747	756(sh)	
$\gamma[N(CH_3)_2]$	528.3	9.6	536	528	
δCNN	454.8	3.3	n.i.	n.i.	
δCNC	367.3	1.0	n.i.	n.i.	
$wN(CH_3)]$	258.7	3.2	n.i.	n.i.	
$\tau(CH_3)as$	223.4	0.1	n.i.	n.i.	
$\tau(CH_3)s$	207.9	0.5	n.i.	n.i.	
γCNN	168.5	1.7	n.i.	n.i.	

[a] Wavenumbers in cm^{-1}; IR intensities in km mol^{-1}. Calculated wavenumbers were scaled by 0.978. , stretching; δ, bending; γ, rocking; τ, torsion; w, wagging; s, symmetric; as, antisymmetric; n.o., not observed; n.i.: not investigated; sh. shoulder.

[b] For furan, α and β designate the carbon atoms alpha or beta in relation to the oxygen atom, and the symbols + and − indicate relative movements of the hydrogen atoms in a given vibration. For DMI, when two types of symmetry are indicated (for methyl groups) the first one refers to methyl group local C_s symmetry and the second one to the molecule global C_s symmetry.

[c] Data for argon matrix.

Conclusions

Matrix isolation IR spectroscopy and DFT(B3LYP)/6-311++G(d,p) calculations allowed the investigation of the structure, infrared spectra and unimolecular photochemistry of 2FDH isolated in solid argon and xenon.

In the molecule, the C=N double bond determines the existence of *E* and *Z* structural isomerism, the *E* form being considerably more stable than the *Z* isomer because of the sterical hindrance between the furyl and $N(CH_3)_2$ substituents and reduced π–p mesomerism in the latter. The internal rotation about the exocyclic C–C bond axis accounts for two different conformers for both *E* and *Z* isomers. The most stable *E*-type conformers (*E*-AG and *E*-SG) differ in energy by 3.5 kJ mol^{-1}, with *E*-AG being the global minimum. The slightly higher stability of the *E*-AG form relatively to *E*-SG results from the presence in the former of a stabilizing weak (N=C–H)···O hydrogen bond type interaction and absence in this form of the destabilizing interaction between the lone electron pairs of the oxygen and nitrogen atoms existing in *E*-SG.

Both *E*-AG and *E*-SG were efficiently trapped from gas phase into cryogenic argon and xenon matrices. Upon broadband UV-irradiation ($\lambda > 328$ nm), the most stable *E*-AG conformer was found to isomerize to form *E*-SG, while irradiation at higher energy ($\lambda > 234$ nm) led to fragmentation of 2FDH into furan and

dimethylisocyanide. The generation of these photoproducts involves the cleavage of the exocyclic C–C bond and simultaneous [1,2] H-atom migration from the $(CH_3)_2$ N═C H moiety to the furyl group. $E \rightarrow Z$ structural photoisomerization of 2FDH was not observed under the used experimental conditions.

Acknowledgements

This work was supported by CYTED (Network 312RT0463), PROMEP (Project UAZ-PTC-092), FCT (Project PTDC/QUI/111879/2009, cofunded by QREN-COMPETE-UE), ANPCyT (PICT(2011)/0226), MinCyT-FCT (Portugal-Argentina bilateral cooperation Grant FCT-MinCyT PO/09/18), MinCyT-CONACyT (Mexico-Argentina bilateral cooperation Grant MX/11/01) and CONACyT (Projects 119491 and 153066). AGZ is member of the Research Career CONICET, Argentina. B.M.G. acknowledges FCT for the postdoctoral grant No. SFRH/BPD/44689/2008.

Appendix A. Supplementary data

Supplementary data associated with this article can be found, in the online version, at http://dx.doi.org/10.1016/j.saa.2012.07.061.

References

[1] N.P. Belskaya, W. Dehaen, V.A. Bakulev, Arkivoc (i) (2010) 275.
[2] S. Kim, J.-Y. Yoon, Sci. Synth. 27 (2004) 671.
[3] R. Brehme, D. Enders, R. Fernandez, J.M. Lassaletta, Eur. J. Org. Chem. 34 (2007) 5629.
[4] S. Dadiboyena, A. Nefzi, Eur. J. Med. Chem. 46 (2011) 5258.
[5] Y.P. Kitaev, B.I. Buzykin, T.V. Troepol'skaya, Russ. Chem. Rev. 39 (1970) 441.
[6] A.M. Wu, P.D. Senter, Nat. Biotechnol. 23 (2005) 1137.
[7] K.T. Potts, B. Walsh, J. Org. Chem. 53 (1988) 1199.
[8] P. Rao, T.N. Pattabiraman, Anal. Biochem. 189 (1990) 178.
[9] S.P. Ivonin, A.A. Anishchenko, M.V. Voevudskii, L.V. Dmitrikova, Chem. Heterocycl. Compd. 34 (1988) 1086.
[10] J. Benites, J.A. Valderrama, F. Rivera, L. Rojo, N. Campos, M. Pedro, M.S.J. Nascimento, Bioorg. Med. Chem. 16 (2008) 862.
[11] K. Bjamer, S. Furberg, C.S. Petersen, Acta Chem. Scand. 18 (1964) 587.
[12] R.H. Wiley, C.H. Jarboe, J. Am. Chem. Soc. 77 (1955) 403.
[13] G. Adembri, P. Sarti-Fantoni, E. Belgodere, Tetrahedron 22 (1966) 3149.
[14] H.C. Barany, E.A. Braude, M. Pianka, J. Chem. Soc. (1949) 1898.
[15] R.W. Layer, Chem. Rev. 63 (1963) 489.
[16] H.S. Seleem, G.A. El-Inany, M.F. Eid, M. Mousa, F.I. Hanafy, J. Braz. Chem. Soc. 17 (2006) 723.
[17] R.W. Binkley, Tetahedron Lett. 23 (1969) 1893.
[18] S.D. Carson, J. Org. Chem. 35 (1970) 2734.
[19] M.J. Frisch, G.W. Trucks, H.B. Schlegel, G.E. Scuseria, M.A. Robb, J.R. Cheeseman, J.A. Montgomery, T. Vreven, K.N. Kudin, J.C. Burant, J.M. Millam, S.S. Iyengar, J. Tomasi, V. Barone, B. Mennucci, M. Cossi, G. Scalmani, N. Rega, G.A. Petersson, H. Nakatsuji, M. Hada, M. Ehara, K. Toyota, R. Fukuda, J. Hasegawa, M. Ishida, T. Nakajima, Y. Honda, O. Kitao, H. Nakai, M. Klene, X. Li, J.E. Knox, H.P. Hratchian, J.B. Cross, V. Bakken, C. Adamo, J. Jaramillo, R. Gomperts, R.E. Stratmann, O. Yazyev, A.J. Austin, R. Cammi, C. Pomelli, J.W. Ochterski, P.Y. Ayala, K. Morokuma, G.A. Voth, P. Salvador, J.J. Dannenberg, V.G. Zakrzewski, S. Dapprich, A.D. Daniels, M.C. Strain, O. Farkas, D.K. Malick, A.D. Rabuck, K. Raghavachari, J.B. Foresman, J.V. Ortiz, Q. Cui, A.G. Baboul, S. Clifford, J. Cioslowski, B.B. Stefanov, G. Liu, A. Liashenko, P. Piskorz, I. Komaromi, R.L. Martin, D.J. Fox, T. Keith, M.A. Al-Laham, C.Y. Peng, A. Nanayakkara, M. Challacombe, P.M.W. Gill, B. Johnson, W. Chen, M.W. Wong, C. Gonzalez, J.A. Pople, Gaussian 03, Gaussian, Inc., Wallingford, CT, 2004.
[20] A.D. Becke, Phys. Rev. A 38 (1988) 3098.
[21] C.T. Lee, W.T. Yang, R.G. Parr, Phys. Rev. B 37 (1988) 785.
[22] A. Császar, P. Pulay, J. Mol. Struct. (Theochem.) 114 (1984) 31.
[23] O. Farkas, H.B. Schlegel, Chem. Phys. 111 (1999) 10806.
[24] H. Rostkowska, L. Lapinski, M.J. Nowak, Vib. Spectrosc. 49 (2009) 43.
[25] P. Pulay, G. Fogarasi, F. Pang, J.E. Boggs, J. Am. Chem. Soc. 101 (1979) 2550.
[26] C. Peng, H.B. Schlegel, Isr. J. Chem. 33 (1993) 449.
[27] C. Peng, P.Y. Ayala, H.B. Schlegel, M.J. Frisch, J. Comput. Chem. 17 (1996) 49.
[28] A.J. Barnes, J. Mol. Struct. 113 (1984) 161.
[29] S.M. Landge, E. Tkatchouk, D. Benítez, D.A. Lanfranchi, M. Elhabiri, W.A. Goddard, I. Aprahamian, J. Am. Chem. Soc. 133 (2011) 9812.
[30] M.N. Chaur, D. Collado, J.-M. Lehn, Chem. Eur. J. 17 (2011) 248.
[31] E. Sánchez-García, A. Mardyukov, M. Studentkowski, L.A. Montero, W. Sander, J. Phys. Chem. A 110 (2006) 13775.
[32] E. Sánchez-García, A. Mardyukov, A. Tekin, R. Crespo-Otero, L.A. Montero, W. Sander, G. Jansen, Chem. Phys. 343 (2008) 168.
[33] N. Kus, I. Reva, R. Fausto, J. Phys. Chem. A 114 (2010) 12427.
[34] A. Mellouki, M. Herman, J. Demaison, B. Lemoine, L. Margules, J. Mol. Spectrosc. 198 (1999) 348.
[35] B. Pankoke, K.M.T. Yamada, G. Winnewisser, Z. Naturforsch. 48 (1993) 1193.
[36] M.P. Bernstein, S.A. Sandford, L.J. Allamandola, Astrophys. J. 476 (1997) 932.
[37] X. Wu, J.L. Stockdill, P. Wang, S.J. Danishefsky, J. Am. Chem. Soc. 132 (2010) 4098.